POLISH POLAR RESEARCH
vol. 47 no. 1–2, pp. 13–26
DOI: 10.24425/ppr.2026.158404

Proglacial zone dynamics revealed with high resolution UAV-based mapping in 2021 and 2023, Renard Glacier, Svalbard

Adrian SZAŁKOWSKI

Institute of Socio-Economic Geography and Spatial Planning, Maria Curie-Skłodowska University, Al. Kraśnicka 2D, Lublin 20-718, Poland

corresponding author: *adrian.szalkowski@mail.umcs.pl*

Received 19 September 2025 **Accepted** 16 June 2026

Abstract: Research on the dynamics of terrain relief changes in the foreland of Renard Glacier (Recherchefjorden, Spitsbergen) provide knowledge about geomorphological processes occurring in Bellsund, one of the biggest fjords in Svalbard archipelago. The aim of the study was to identify and characterize contemporary geomorphological transformations in the marginal zone of the glacier, resulting from intensive ice melting, with particular emphasis on the dynamics of changes within the tidal flat. Research material was obtained in 2021 and 2023 using an unmanned aerial vehicle (UAV). Advanced photogrammetric techniques were applied, including Agisoft Metashape Pro software, to develop a Digital Elevation Model and orthophotomap with exceptionally high resolution of 0.1 m/px. In addition, the mean annual retreat rate of glacier was estimated at 11.17 m yr^{-1}. The obtained data enabled terrain analysis with unprecedented detail, allowing for precise mapping of changes occurring over short time intervals. The greatest transformations were identified in the active zone at the glacier terminus, where melting ice generates significant amounts of water, intensifying transport processes and redeposition of material to further parts of the fluvial fan.

Keywords: Arctic, Spitsbergen, glacier, geomorphology, unmanned aerial vehicle.

Introduction

Rising average air temperature, declining sea ice cover, and intensification of glacier melting and permafrost thawing are the main manifestations of global warming in polar regions (Barry 2017; Biskaborn *et al.* 2019; Ballinger *et al.* 2020; Sumata *et al.* 2023). These processes lead to significant environmental transformations, including erosion, transport and accumulation of rock material, particularly in proglacial zones (Ewertowski and Śledź 2022). Areas located in glacier forelands, are dynamically shaped by meltwater with high erosional potential, resulting in the formation of fluvioglacial landforms such as outwash plains, eskers or deltas (Rachlewicz 2009; Kavan and Strzelecki 2023). In Svalbard, the widespread retreat of glaciers since the end of the Little Ice Age has become a principal driver of contemporary landscape change, progressively transforming a glacially dominated terrain into a paraglacial one that reaches from the newly deglaciated forefields to the coastal zone (Kavan and Strzelecki 2023). Along the fjords, the recession on tidewater glaciers continually exposes new stretches of coastline, as exemplified by Brepollen in Hornsund, one of the youngest bays of Svalbard, whose shores have developed a variety of paraglacial landforms, including deltas, cliffs, tidal flats and beaches, over the past century (Strzelecki *et al.* 2020). Where meltwater streams draining the glaciers reach the fjord, they build glacier-fed deltas whose development is closely coupled to the glacifluvial sediment supplied by the retreating ice (Mercier and Laffly 2005; Strzelecki *et al.* 2018). Inland of the coast, the freshly exposed forefields evolve into highly dynamic systems in which meltwater continuously erodes, transports and redeposits glacigenic sediment, so that individual landforms may be reshaped even within a single ablation season (Rachlewicz 2009; Zagórski 2011).

The forefield of Renard Glacier (Spitsbergen) is an example of a proglacial environment where a combination of melting ice and precipitation shape a new landscape. Previous research based on satellite imagery and ground measurements, due to limited spatial resolution (< 0.5 m), did not allow capture the spatial variability of processes in the glacier's marginal zone (Reder 1996; Zagórski 2011). In response to these limitations, unmanned aerial vehicles

(UAV) combined with Structure-from-Motion (SfM) technique are gaining increasing importance. These methods enable the generation of high-resolution Digital Elevation Models (DEM) and orthophotomaps, filling the gap between traditional ground-based research and satellite remote sensing (Tonkin and Midgley 2016; Chandler *et al.* 2018; Śledź *et al.* 2021).

The aim of this study was to analyze geomorphological transformations in the foreland of Renard Glacier in 2021 and 2023, with particular emphasis on the zone at the glacier terminus. The research included the generation of Digital Elevation Models, orthophotomaps and followed by the identification of morphological forms and creating maps using UAV data with 0.1 m/px resolution. AgEagle eBee X drone with Aeria X camera was used for data acquisition, and analyses were conducted using Agisoft Metashape, ArcGIS Pro and GlobalMapper software. Flights were performed during the polar day period (July–August in 2021 and 2023), which allowed for obtaining detailed data exceeding the accuracy of available satellite imagery. The results provide new information about fluvioglacial processes and their impact on terrain relief, enabling precise monitoring of proglacial environment dynamics in the area of Renard Glacier.

Study Area

The Svalbard Archipelago, located in the northern part of the Arctic Ocean, covers an area of 60,299 km². Its largest island is Spitsbergen (39,044 km²), first documented by Willem Barentsz in 1596, located in the northwestern corner of the Barents Sea shelf, on the edge of the Eurasian continental plate, opposite the Greenland plate (Johnson and Heezen 1967; Birkenmajer 1972). Spitsbergen's climate is shaped by the warm West Spitsbergen Current, a branch of the Gulf Stream, which moderates winter temperatures and influences thermal differences between the island's interior and coastal areas (Walczowski and Piechura 2011; Kostrzewski and Zwoliński 2013).

Bellsund strait, located in the northwestern part of Wedel Jarlsberg Land, between the Dunder valley and Recherchefjord, encompasses a mountainous area of approximately 360 km², dissected by glaciated valleys (Stankowski *et al.* 2013). Within the bay is Renard Glacier, covering 28 km² (down from 38 km² in 1936), with a length of 8 km and width of 2.7 km. Since the 1990s, the glacier terminus has not reached the shoreline of Recherchefjord, resulting from its recession under Arctic climate warming conditions (Biskaborn *et al.* 2019; Dobiński and Kasprzak 2022).

The forefield of Renard Glacier (Fig. 1) is a classic proglacial environment, characterized by diverse geomorphological forms such as sedimentary fans, outwash plains and water pools, shaped by glacial and periglacial processes (Reder and Zagórski 2007; Zagórski *et al.* 2008). Intensive ice melting and fluvial flows lead to erosion, transport and accumulation of rock material, particularly in the glacier's marginal zone, where fluvioglacial forms dominate (Rachlewicz 2009).

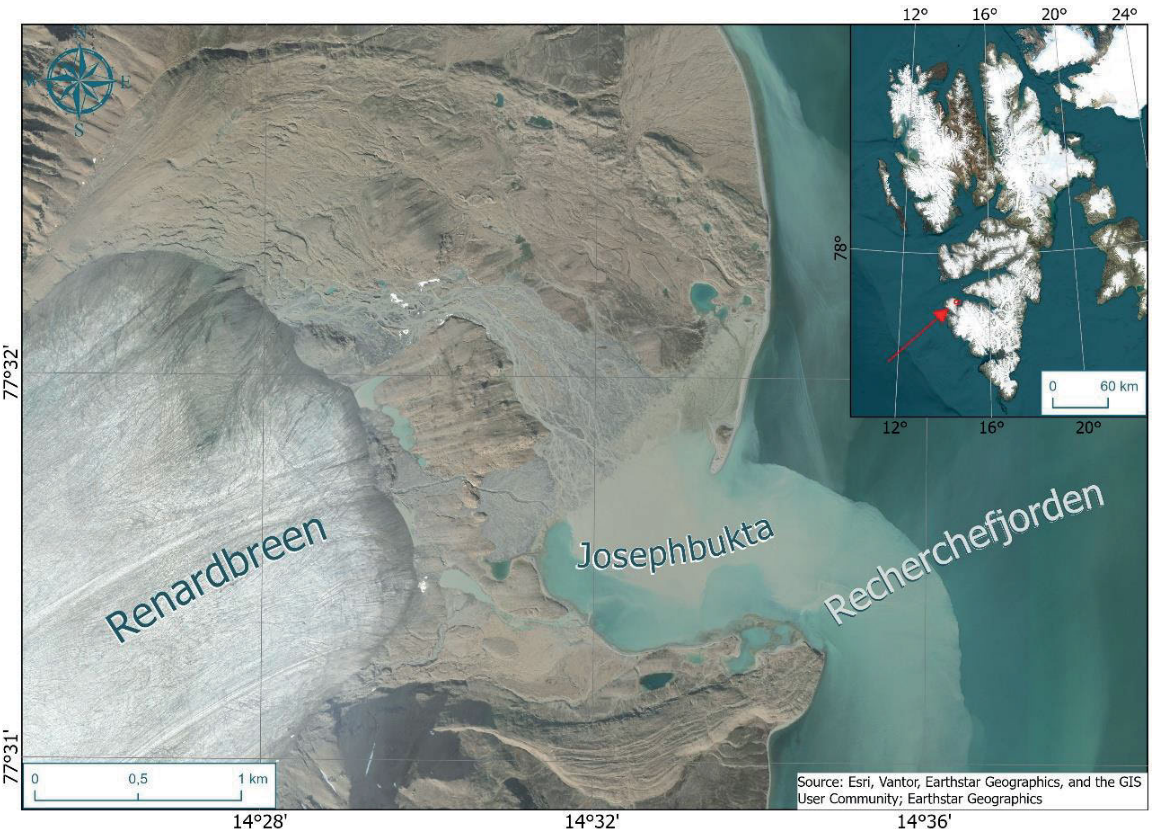

Fig. 1. Location of the Renard Glacier and its forefield; data provided by ESRI (2023).

The Renard Glacier catchment covers 41 km², of which 73% (29.88 km² measurements from 2023) is occupied by the glacier. Meltwater, mainly supraglacial, feeds the foreland, creating pools and streams with high discharge dynamics during the summer period (June–September). Proglacial runoff constitutes up to 90% of total runoff during the ablation season, with rapid ablation-rainfall floods (Bartoszewski 1998; Killingtveit *et al.* 2003). Glacier drainage occurs through three pathways: supraglacial, englacial and subglacial, with a network of meandering channels and glacial portals 2–3 m high. Meltwater transports sediments, mainly medium gravel, and the lack of direct surface runoff (Pękala *et al.* 2013). During winter, icing covers persist on the foreland, indicating the glacier's hydrological activity (Zagórski *et al.* 2012). Genetically, waters on the foreland originate from supraglacial, supra permafrost and rainfall sources, with proglacial waters dominating in glaciated catchments.

Temperature data for the study area were obtained from the Akseloya Meteorological Station (77.6914°N, 14.7746°E) (YR.no, Norwegian Meteorological Institute), which is the closest weather station to Renard Glacier, *ca*. 20 km from the station. The study area is characterized by Arctic climate conditions with pronounced seasonal temperature variation. Mean air temperature during the winter period (November-March) remains below −6°C with March being the coldest month, recording a mean temperature of −10.1°C and minimum values down to −23.2°C. The annual temperature amplitude amounts to approximately 30°C. The glacier ablation season is concentrated in the June-August period, when mean temperatures exceed the freezing point (Figs. S1 and S2).

Detailed monthly temperature records for 2021 and 2023 observation periods from the Akseloya station are presented in Figs. S1 and S2, respectively, showing maximum, mean and minimum temperatures. The pronounced seasonality in temperature regimes directly influences the intensity of glacier ablation processes and snowmelt dynamics in the proglacial zone. The transition months of May-June and August-September are particularly critical for meltwater generation, as they represent periods of rapid temperature increase and decrease, respectively, significantly affecting sediment transport and landform development in the proglacial area.

Materials and methods

Fieldwork was conducted during the summer season (July–August) in 2021 and 2023, under polar day conditions. The study area covered 6 km². The survey began with the placement of Ground Control Points (GCPs), using easily identifiable stones or wooden boards arranged in a cross pattern and marked with geodetic paint. GCP position measurements were taken using a Topcon HiPer HR GNSS receiver with a Topcon FC-6000 controller, with georeferencing accuracy based on a geoid height of 33.4554 m. All points were recalculated at the base of the reference point in Calypsobyen (CALY point). In 2023, additional GCPs were prepared on the glacier forefield, reducing the distances between them to increase positional precision. Finally, 90 GCPs were established and utilized during the photogrammetric processing stage.

Photogrammetric surveys were carried out at 250 m above the ground level using an AgEagle eBee X unmanned aerial vehicle (UAV) equipped with an RTK/PPK GNSS receiver and an AgEagle Aeria X camera. Flight missions were planned using eMotion software, with 70% image overlap for vertical shots. Over 50 GB of imagery data were collected, with a total of 11,467 images acquired during the 2021 and 2023 polar expedition. The size of one photo is from 7 MB to 10 MB with dimensions of 6000x4000, 24 MP. The coordinate system used for processing was WGS 84 / UTM Zone 33N (EPSG: 32633), orthometric heights refered to Svalbard Vertical Datum 2006 at https://epsg.io/1323-datum.

During ground control point (GCP) acquisition, the number of available satellites typically reached 28 throughout the observation period. The real-time kinematic (RTK) positioning status was consistently maintained at fixed throughout all measurement operations. Horizontal positional accuracy (H) during measurements remained within ±1 cm, while vertical accuracy (V) typically achieved ±2 cm. Figure S3 illustrates a representative example of the receiver information display captured during GCP measurement operations.

The Topcon FC-6000 rover receiver antenna was positioned at a constant height of 2 m above terrain using a surveying pole. The fixed antenna height was maintained consistently through all 90 GCP measurements. Each measurement location was held steady for 10 seconds to allow convergence of the RTK solution.

Photogrammetric data were processed in Agisoft Metashape Professional (version 2.0.3, build 16960), resulting in the generation of orthophotos, Digital Elevation Models (x 0.1 m, y 0.1 m) (DEMs), and point clouds with a resolution of 0.1 m/px. Geomorphological forms were vectorized based on the 2023 orthophoto, supplemented by source materials such as the Geomorphological Map of the Renard Glacier Forefield (Bartoszewski *et al.* 2003) and the Glacial Landform Interpretation Map of Renard Glacier (Szczęsny *et al.* 1989). The vectorization process was guided by literature on geomorphological features. Based on the DEM, contour lines were generated for the 20–80 m elevation range at 20 m intervals, and active watercourses were delineated. Spatial analyses and data validation were performed using ArcGIS Pro and GlobalMapper, synchronizing data across the three years using GCPs. Data processing was carried out on a high-performance workstation to ensure the high quality of output data. Additional information generated during the creation of the orthophotomap and DEM is presented in Table 1.

Glacier terminus positions were extracted from high-resolution orthophotomaps acquired during the 2021 and 2023 UAV campaigns through manual digitalization. The terminus was defined as the contact between active glacier

Table 1. Parameters, accuracy and RMSE errors of measurements taken using an unmanned aerial vehicle (UAV), as well as the Digital Elevation Model (DEM) and orthophoto map. Report generated in Agisoft Metashape.

GCPs	90
Coverage area (km)	6
Height of UAV flight AGL (m)	250
Photos	11,467
Photo res.	24 MPx
Avg. Size of photo	*ca.* 9MB
X size of DEM (m)	0.1
Y size of DEM (m)	0.1
X size of Orthophotomap (m)	0.1
Y size of Orthophotomap (m)	0.1
RMSE errors	
RMSE total error (cm)	3.36
X error (cm)	1.88
Y error (cm)	2.13
Z error (cm)	1.8
Coordinate system	WGS 84 / UTM Zone 33N

ice and debris-covered ice or proglacial sediment. Terminus polylines were digitized in ArcGIS Pro.

To quantify spatial variability in retreat rates across the glacier width, a systematic transect based approach was employed. Perpendicular transects were generated at regular 90 m intervals orthogonal to the approximate trend of the glacier terminus. Retreat distance from each transect was calculated as the perpendicular distance between the 2021 and 2023 terminus positions. The approach provided multiple independent retreat measurements distributed across the entire glacier front, enabling quantification of both mean retreat rates. For temporal context, archived orthophotomap from 2011 (Norwegian Polar Institute, NP Ortofoto Svalbard WMTS 25833) was used and processed using identical digitalization and analysis procedures to quantify longer-term (2011–2021) terminus change. All figures presented in this section below were taken by the author using a UAV in 2023 during the XXXI UMCS Polar Expedition.

The obtained geomorphological map of the Renard glacier foreland allowed identification of fourteen types of formations. (1) Tidal flat is a coastal area that is regularly flooded and exposed by marine tides. Plain is typically flat and extend from the shoreline to where water depth begins to increase rapidly. Tidal sediments, such as silt and sand, are the main materials building the tidal flat. (2) Contemporary stormy bar (beach) is quite narrow and occurs mainly at the spit and in the southern part of the foreland, adjacent to the bay. A storm ridge is also located on it. (3) Terrace is located at the end of the spit headland and reaches a height of up to 2 meters. (4) Outwash plain (inactive outwash plains) occur near the formed lateral moraines, where glacial water flowed in previous years. These extensive plains are built of sands and gravels that were deposited by glacial waters, but are currently not actively formed by contemporary hydrological processes. (5) The fluvial cone (Fig. 2) is the most active and dynamic landform in the studied glacier forefield. In this area, meltwater drains the substrate and accumulates material. Alluvial fans form where glacial meltwater flows onto flatter terrain, depositing transported sediments in a fan-shaped pattern similar to a delta. (6) Eskers (Fig. 3) are long, narrow ridges composed of sands and gravels, formed by the deposition of sediment from glacial meltwater flowing through subglacial tunnels. In the glacier forefield, they developed prior to 1960 as well as between 1995 and 2005, during periods of glacial retreat. (7) A kame terrace is a flat or gently sloping surface composed of moraine material. It forms as a result of the melting of dead ice that remains buried under sediments, creating characteristic terraces along the slopes of glacial valleys. (8) The glacier is continuously undergoing ablation, with numerous crevasses on its surface. Ablation includes the melting and sublimation of ice, leading to a reduction in the glacier's mass and size. (9) A Roche Moutonnee (Fig. 4), is a distinctive landform created by glacial erosion. It consists of smooth, rounded bedrock ridges shaped by the movement of ice, giving them a wavy, asymmetrical form—with a gentle slope facing the glacier front and a steep scarp on the opposite side. (10) A Ground moraine is located directly beneath a glacier and becomes exposed as the glacier melts. It consists mainly of sands, gravels, and clays that have been eroded from the bedrock by the moving ice. Ground moraines clearly illustrate the former extent of the glacier front in previous years, especially when glacial meltwater begins to meander through them. (11) An ablation moraine consists of glacial deposits left behind as the glacier melts. These sediments often form hummocky or irregular landforms, containing a wide range of materials from fine silts to large boulders. On the map, hummocky areas within the ground moraine zone have been marked as ablation moraines. (12) A lateral moraine forms as a result of material accumulating along the sides of a glacial valley. The debris pushed by the glacier marks the maximum extent of the ice. Numerous small lakes can form on the lateral moraine, sustained by permafrost and remnants of dead ice embedded within the moraine. (13) A terminal moraine (Fig. 5) is a ridge of sediments that forms at the front of a glacier. It develops as the glacier pushes rocky material toward its terminus and then deposits it as the ice melts. It is characterized by folding and is located on the outer edge of the glacier. (14) Glacial ice ponds are a result of ice melting, which creates depressions in the terrain that are subsequently filled with water. These can be proglacial lakes, which develop in natural depressions, retaining water from the melting glacier and precipitation.

Fig. 2. Alluvial fan on the forefield of the Renard glacier; photo from 2023 oriented toward the Josephbukta bay.

Fig. 3. Eskers in the central part near the glacier front on full view (upper panel) and in zoom (lower panel); photo from 2023 oriented northward.

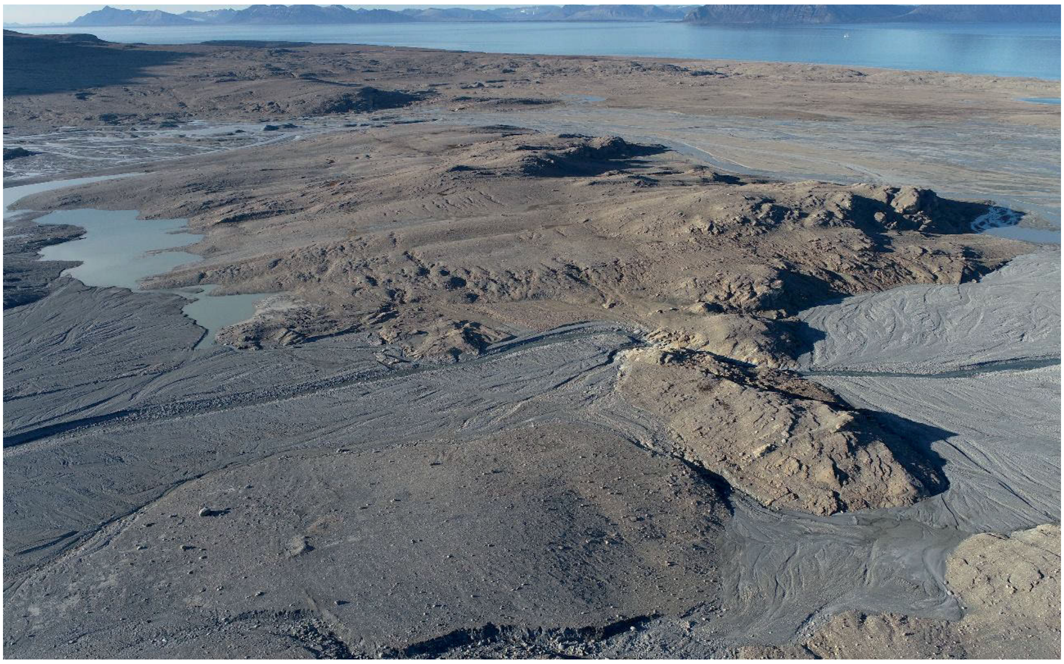

Fig. 4. Roche moutonnee in the central part under the eskers; photo from 2023 oriented northward.

Fig. 5. Terminal moraine, photo from 2023 taken towards Reinholmen.

Glacier Terminus Retreat Rates

Glacier terminus changes were quantified using orthophotomaps from 2021 and 2023. Glacier extents were manually digitized, enabling the application of the Generate Transects Along Lines (Esri ArcGIS Pro, Linear Referencing toolbox) to produce transects connecting corresponding sections of the terminus between the two time periods. The generated transects were subsequently clipped to the glacier front in order to derive actual retreat distances. A constant spacing between transects was applied to ensure uniform spatial sampling. A quality control procedure was conducted to remove transects with incorrect orientation relative to the glacier front, as these could artificially inflate retreat distances. Consequently, the number of transects differs from that used in the 2011–2021 analysis. The spatial arrangement and geometry of transects are illustrated in Fig. 6.

Results

Paraglacial morphodynamic zones are areas undergoing intense geomorphological transformations due to glacier mass loss. Based on photogrammetric data from the Renard Glacier forefield, paraglacial morphodynamic zones were delineated. Meltwater from the glacier induces ero-

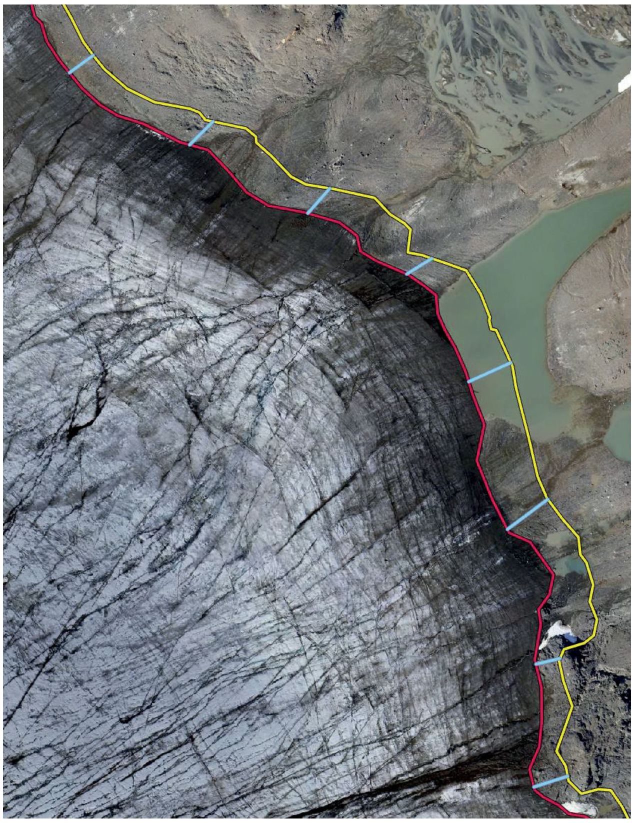

Fig. 6. Change in extent of part of the glacier front between 2023 (in red) and 2021 (in yellow). The blue lines represent the transects discussed in section Glacier Terminus Retreat Rates.

sion, transport, and deposition of sediment, contributing to the development of diverse landforms such as glacially polished surfaces, Roche Moutonnée, and ground moraines. A new geomorphological map of the glacier forefield was developed (Fig. 7), updating the data from the previous map published in 2003 (Bartoszewski *et al.* 2003). This allowed for the identification of new landforms and the assessment of dynamic changes in the glacier's marginal zone. All figures presented below were created by the author using ArcGIS Pro.

Beyond the qualitative inventory of those landforms, the high-resolution ortophotomaps also allowed the rate of change of the glacier itself to be quantified. Because the position of the terminus exerts a first-order control on the delivery of meltwater and sediment to the forefield, the magnitude and across-front variability of frontal retreat were measured directly from the digitized 2021 and 2023 ice margins and for longer-term context, from archival imagery acquired in 2021, see Materials and methods.

Analysis of the 2021–2023 (Fig. S4) indicates a mean terminus retreat of 22.34 m over the two-year period, corresponding to a mean annual retreat rate of 11.17 m yr^{-1}. Transect-based retreat distances range from 7.29 m to 43.57 m, highlighting substantial spatial variability across the glacier front. To place recent changes in a longer-term context, a decadal-scale analysis was conducted using archived orthophotomaps. Results for the 2011–2021 period (Fig. S5) show a cumulative terminus retreat of 144.58 m, corresponding to a mean annual retreat rate

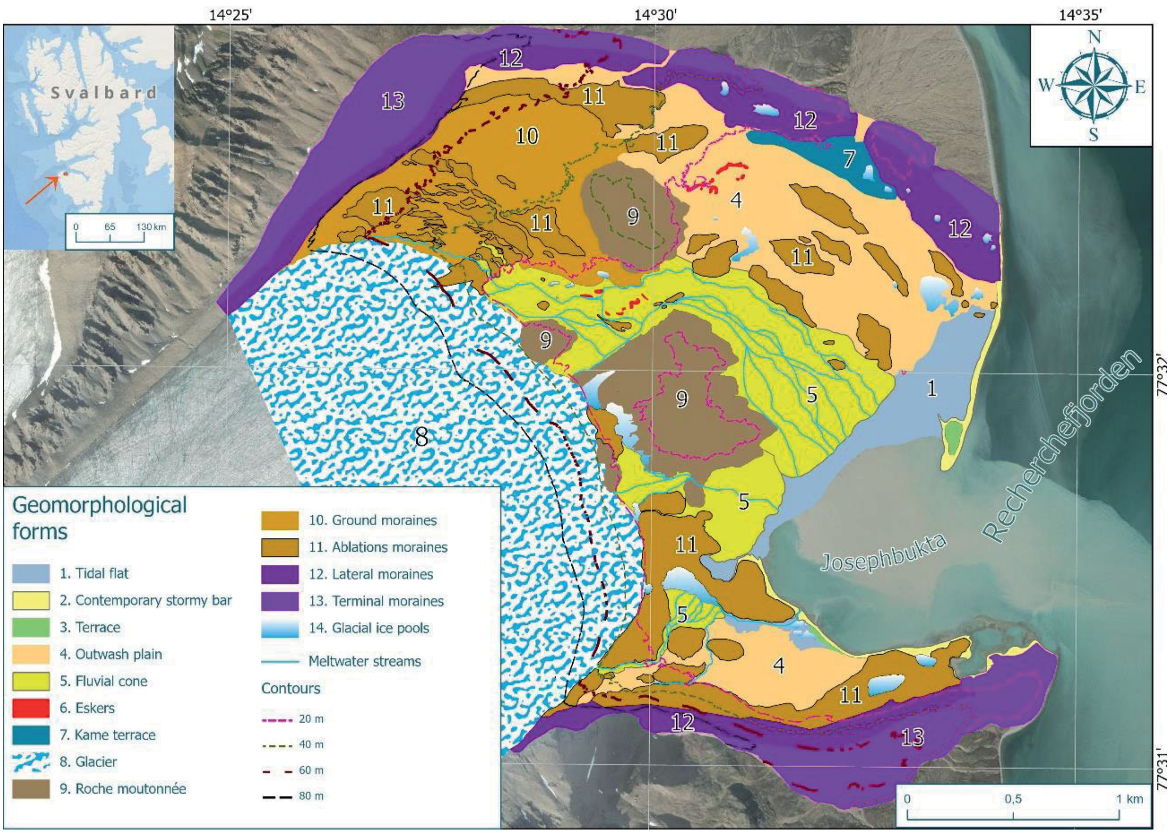

Fig. 7. Geomorphological map of Renard Glacier forefield, based on an orthophotomap generated in 2023 with a UAV, supported by maps from Szczęsny *et al.* (1989) and Bartoszewski *et al.* (2003).

of 14.46 m yr⁻¹. Retreat distances during this period range from 44.7 m to 225.6 m, indicating pronounced variability in glacier response over time.

Comparison of Digital Elevation Model Results

The use of Digital Elevation Models (DEMs) enables detailed analysis of topographic changes in glaciers and their drainage systems. Below, the analyzed changes in the extent and drainage of the Renard Glacier in Spitsbergen between 2021 and 2023 are presented, based on a comparison of rasters from these years (Fig. 8). It is important to emphasize that the DEMs allowed detection of even the smallest changes, thanks to their 10-centimeter resolution. Calculating the changes between the two rasters was possible through the use of the Raster Calculator in ArcGIS Pro software.

Comparison of Digital Elevation Models (DEMs) from 2021 and 2023 reveals strong spatial heterogeneity in surface elevation changes across the Renard Glacier forefield (Fig. 8). The area-averaged ice-surface lowering between August 2021 and August 2023 is approximately −2.6 m, but this signal is highly variable: the most negative values (up to −9.0 m) occur in a single, narrow location corresponding to the blue color on the legend. This site marks a deep incision, *i.e.*, a supraglacial drainage channel cut into the glacier by meltwater flowing from the ice. The channel depth was not measured independently; the −9.0 m value was derived from the high-resolution (10 cm) DEM acquired during UAV-based terrain mapping. These features represent local incision of the ice surface (channel depth relative to the surrounding ice) rather than uniform lowering of the glacier snout, and the −9.0 m value should be interpreted as the maximum channel depth, not as a mean elevation change. Local accumulation reaches more than 1.6 m elevation gain elsewhere on the foreland. Adjacent to the glacier terminus, the northern sector near the lateral moraine exhibits substantial sediment accumulation (elevation gain of 1.5 m), attributed to the combined effects of river sediment deposition by melting water and slope processes transforming glacial material. This dual-origin accumulation highlights the transition zone where erosional products from the retreating ice margin are rapidly redeposited.

Central meltwater pathways have formed ground moraines that evolve into inactive sandurs due to declining hydrological connectivity. These sandurs now show minimal elevation change (±0.2 m), indicating landscape stabilization. Downstream, beyond fluted moraines, sediment is actively remobilized and transported toward Josephbukta strait, with denivelations of up to 1 m, typically *ca.* 0.7 m. Here, sandur cones undergo erosion, while the distal delta region exhibits sediment washout. A well-braided alluvial fan system in the lower southern margin records significant sediment transfer (elevation gain of 1.6 m) from upper terminal areas over the two-year period, with material transported beyond a dissected ground moraine.

Notably, minor positive elevation changes (elevation gain of 0.20 m) between fluted moraines likely reflect transient snow accumulation in 2023 rather than sediment dynamics. Relict meltwater channels along lateral mor-

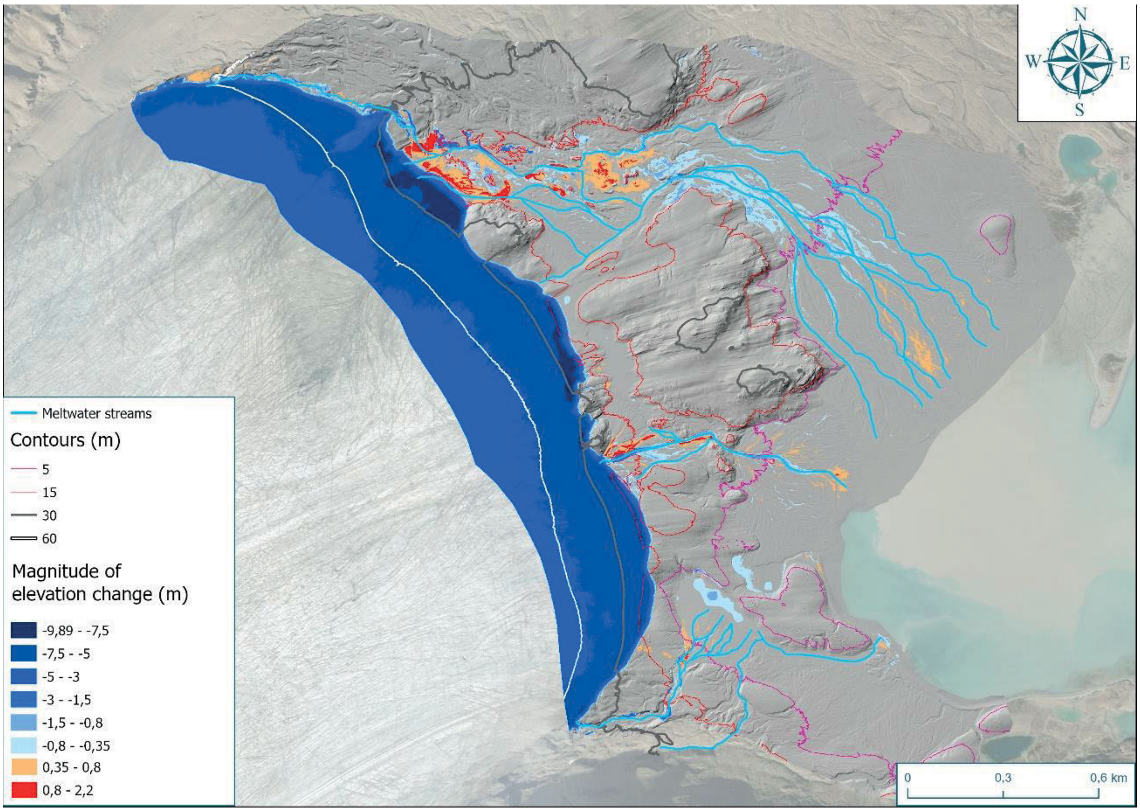

Fig. 8. Differences between Digital Elevation Models created for 2021 and 2023.

aines, active in prior years but now abandoned, further attest to shifting drainage patterns as the glacier retreats. The forefield thus exemplifies a paraglacial sequence: channel-confined meltwater incision of the ice surface, locally reaching elevation loss of 9.0 m, feeds proximal depositional systems (elevation gain of 1.5 m), while distal zones undergo gradual reworking through fluvial export (elevation loss of 1.0 m) and deltaic adjustment.

This integration of elevation data and geomorphic context confirms that the 1.5-meter accumulation zone represents a dynamic interface where both fluvial processes (meltwater sediment transport) and slope processes (moraine collapse, debris redistribution) interact to build relief. Concurrently, the transition of active sandurs to inactive states, marked by sediment exhaustion and absent hydrologic recharge, illustrates the rapid decoupling of glacial sediment sources from proglacial landscapes during retreat.

Outside the supraglacial drainage corridors discussed above, the elevation changes between 2021 and 2023 (Fig. 8) are comparatively modest and mostly relate to reorganisation of the meltwater stream network: in 2023 water was routed predominantly through channels established the previous year. The mean ice-surface lowering of the glacier itself, averaged across the snout, was approximately −2.6 m over the two-year interval, an order of magnitude smaller than the maximum channel-incision values reported above.

Ground moraine zones

Identified on the 2023 orthophotomap occur in several places on the glacier forefield. In the northern part, the moraine position is inclined toward the central (southeastern) direction, which significantly affects the formation of moraine incisions. Flowing glacial water transports loose material (sands, gravels) located in front of the glacier's terminus, carrying it to the lower parts of the forefield. Figure 9 shows the retreated glacier front, in front of which the ground moraine is exposed. When the glacier remains in the same place for a longer period, waters flowing over it create new incisions mentioned above. Over time, ground moraines will become inactive due to lack of water supply and will only be subject to the weathering process, as well as serve as channels draining melting snow.

Changes in the proximal slope of the moraine

Changes within the proximal slope of the moraine are not significant. They occur in the section adjacent to the glacier terminus, as shown in Fig. 10 through a comparison of the same area on 2021 and 2023 orthophotomaps. Most differences relate to the expansion of the glacial ice pools, which is enlarging its surface area into terrain exposed by glacier retreat. Here, the substrate has low permeability and slopes towards the glacier, resulting in the accumulation of meltwater in this location.

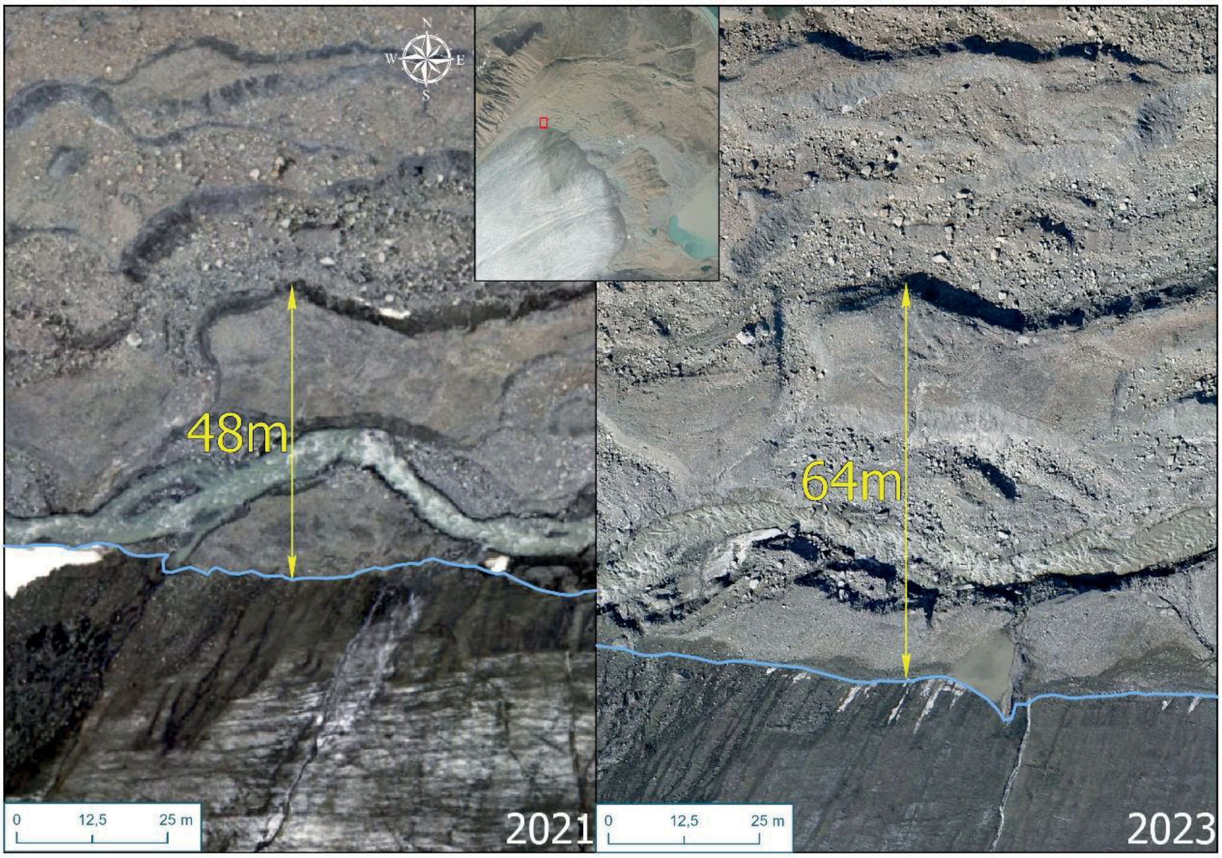

Fig. 9. Exposed ground moraine shaped by a meandering stream. The glacier extent is marked in blue. The additional map in the central part shows the glacier forefield, while the red square represents the exact extent of the area being depicted, 2023.

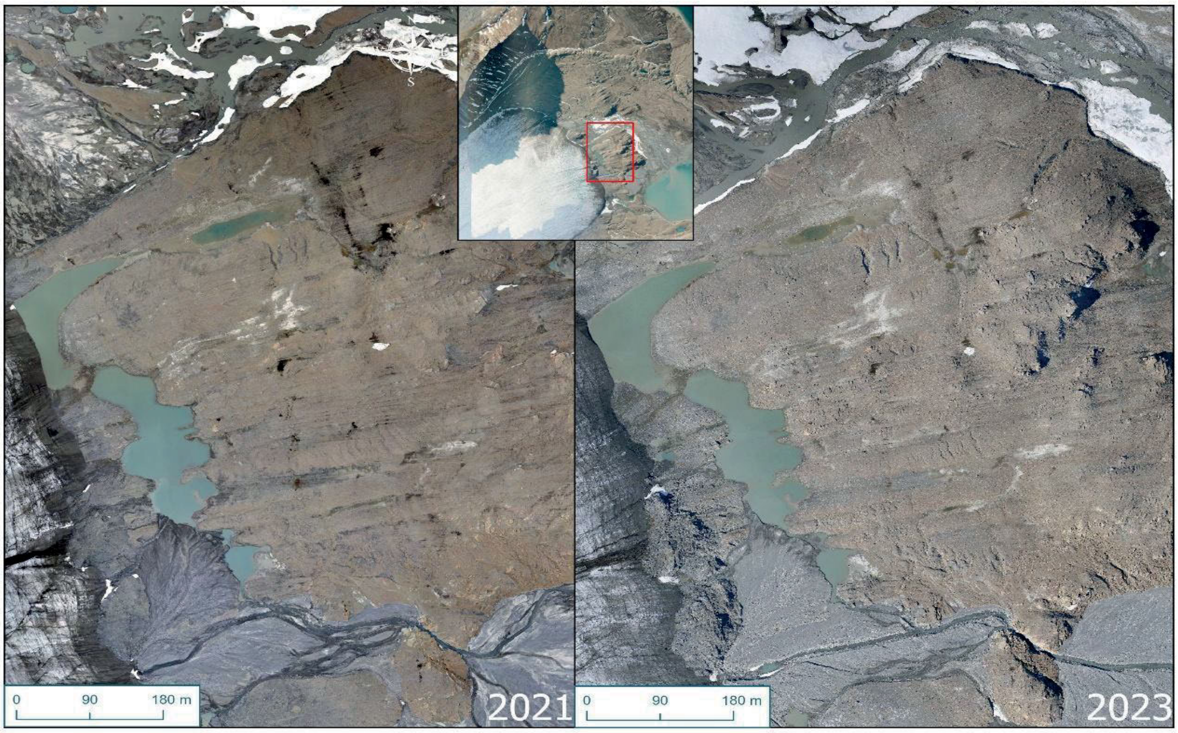

Fig. 10. Difference within the proximal slope of the mutton (Rochee moutonnee). The additional map in the central part shows the glacier forefield, while the red square represents the exact extent of the area being depicted, 2023.

The southern moraine slope exhibits rapid drainage reorganization, with meltwater abandoning distributary channels to form a single-thread, high efficiency outlet through the incised Rochee Moutonnee. This channel simplification likely reflects either a high magnitude discharge events overriding previous flow paths, or cryogenic obstructions (stagnant ice/snow) redirecting flow.

Sandur Zones

The most significant geomorphic changes within Renard Glacier's foreland occur in the sandur zone. Substantial meltwater discharge through this area drives intense terrain reconfiguration, as documented in Fig. 11. Orthoimagery reveals a 48% reduction in feature width, from 79 m in August 2021 to 41 m in August 2023 (Fig. 11), reduction in area by almost 70% from 4808.2 m^2 to 1382.3 m^2 and by 2043 m^3 in volume. This rapid morphological change demonstrates exceptionally high sediment remobilization rates (*ca.* 19 m yr^{-1}), indicative of dynamic proglacial landscape evolution. These observations align with Pękala *et al.* (2013), who documented vigorous erosion in Renard Glacier's environment primarily through proglacial rivers that dissect the sandur plain, fragmenting it into isolated sediment patches and sediment islands, Fig. S6 showing more detailed changes.

Coastal Zone Dynamics

The coastal zone of Renard Glacier foreland occupies its eastern margin, adjacent to Josephbukta strait, where the proglacial river discharges (Pękala *et al.* 2013). Figure 12 documents changes in the southern littoral sector. While orthoimagery reveals substantial geomorphic reconfiguration, distinguishing between glacial-fluvial and marine wave influences remains challenging. Meltwater transports sediment that accumulates at channel mouths, where distributary systems continually reshape the coastline through erosion-deposition feedbacks. Concurrently, wave action undercuts shores and reworks sedimentary deposits. As noted by Mercier and Laffly (2005) and Strzelecki *et al.* (2018), such deltas represent Svalbard's most abundant modern coastal landforms, evolving through sediment supply from both glacial and non-glacial streams.

Discussion

When the present results are placed against the regional pattern of paraglacial evolution, the Renardbreen foreland records a transitional stage in which active glacial geomorphic processes (frontal retreat, ice-marginal sedimentation, ablation moraine collapse) coexist with an emerging paraglacial overprint (sandur reworking, marine undercutting, channel fragmentation, kettle-pond expansion). Such coupling of glacial recession with rapid paraglacial coastal response has been documented across southern Spitsbergen. In Brepollen, six tidewater glaciers have produced more than a hundred kilometers of newly exposed paraglacial coast within the last century (Strzelecki *et al.* 2020), at Gasbreen the development of an ice-dammed lake has fundamentally re-organised sediment-transfer pathways (Dudek *et al.* 2023), and along the Svalbard archipelago retreat of glaciers is a main driver of the for-

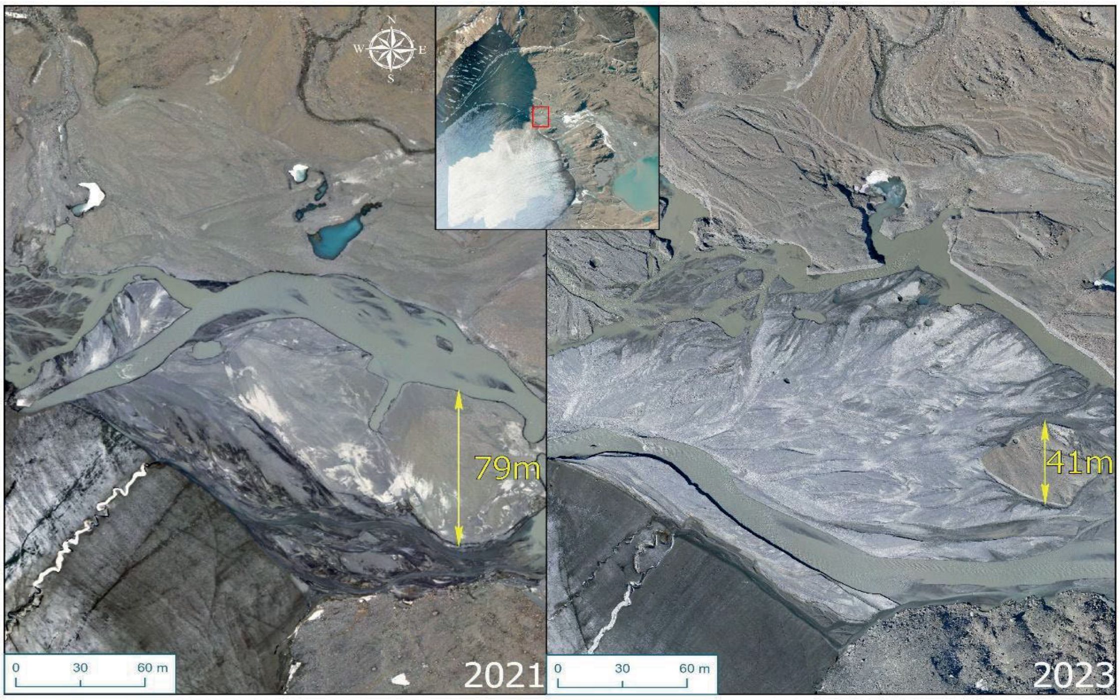

Fig. 11. Morphological transformation of sandur feature between 2021 and 2023. Width reduction from 79 m to 41 m reflects intense fluvial dissection. The additional map in the central part shows the glacier forefield, while the red square represents the exact extent of the area being depicted.

Fig. 12. Coastal morphology between 2021 and 2023 showing proglacial delta with active distributary channel. Sediment plumes indicate ongoing delivery of glaciogenic material. The additional map in the central part shows the glacier forefield, while the red square represents the exact extent of the area being depicted, 2023.

mation of new Arctic coastal environments (Kavan and Strzelecki 2023). Within this framework Renardbreen, only recently uncoupled from the sea, can be regarded as a present-day analogue of the paraglacial evolution already advanced in Hornsund and Sørkapp Land, but at an earlier stage of post-tidewater readjustment. The high-resolution baseline established for 2021–2023 therefore has predictive value for the next generation of land-terminating glacier forelands in western Spitsbergen.

The mean terminus retreat of Renardbreen reconstructed for 2021–2023 (11.17 m yr^{-1}; transect range 7.3–43.6 m yr^{-1}) is *ca.* 23% lower than the 2011–2021 decadal mean (14.46 m yr⁻¹). The 2023 endpoint corresponds to mid-summer orthophotography, so further retreat is to be expected before the end of the ablation season, and the across-front variability documented in Figs. S4–S5 indicates that local controls on basal hydrology and bed topography are at least as important as the climatic forcing in setting the inter-annual signal at Renardbreen. Placed in the regional context, the values measured here lie at the lower end of the southern-Spitsbergen spectrum. Tidewater glaciers in Hornsund retreated on average at *ca.* 70 m yr^{-1} during 2001–2010, markedly faster than the Svalbard archipelago mean of *ca.* 45 m yr^{-1} (Błaszczyk *et al.* 2013). Strzelecki *et al.* (2020) document that recession of six tidewater glaciers in Brepollen has produced more than 100 km of newly exposed paraglacial coast within the last century. The foreland of Gåsbreen (Sørkapp Land) more than doubled in area between 1938 and 2020 in response to a post-1990 acceleration of recession (Dudek *et al.* 2023). The Svalbard-wide synthesis based on 124 919 calving-front positions of 149 marine-terminating glaciers shows that more than 90% of these ice masses retreated between 1985 and 2023, with the western coast, where Renardbreen is located, exhibiting a stronger ocean-warming control than the east (Li *et al.* 2025). The comparatively moderate Renardbreen rate is therefore consistent with its ongoing transition from marine- to land-terminating dynamics; once the calving margin had been lost in the 1990s (Pękala *et al.* 2013), frontal retreat became governed primarily by surface ablation rather than by ocean-driven calving, a behaviour widely reported elsewhere on Svalbard (McCerery *et al.* 2025; Li *et al.* 2025).

The Digital Elevation Model of Difference analysis (Fig. 8) resolves a coupled erosional–depositional system: against a mean ice-surface lowering of *ca.* −2.6 m, channel-confined incision of the ice surface exceeds 9 m within narrow supraglacial drainage corridors and the immediate frontal zone, and is balanced by accumulation of more than 1.5 m on the proximal sandur and along the lateral moraine, while the distal delta is being incised at decimetric rates. This pattern is the geomorphic signature of a polythermal Svalbard foreland in which proglacial runoff supplies up to 90% of total catchment discharge during the ablation season (Bartoszewski 1998; Killingtveit *et al.* 2003), and is fully consistent with earlier descriptions of vigorous fluvial dissection of the Renardbreen sandur (Reder 1996; Reder and Zagórski 2007; Zagórski 2011). The same dual signature of marginal accumulation and channel-bound erosion has been documented in comparable UAV-SfM surveys at Austre Lovenbreen (Bernard *et al.* 2017) and Horbyebreen (Ewertowski *et al.* 2019a) The 48% width reduction of the active sandur feature from 79 m to 41 m between 2021 and 2023, and mass loss of the selected moraine remnant by 2 043 m^3 provide quantitative confirmation that fluvio-glacial reworking is currently the principal control on sediment redistribution in the Renardbreen foreland.

The processing chain, *i.e.*, RTK-GNSS GCPs, Agisoft Metashape and a workflow checked against ArcGIS Pro and GlobalMapper, follows the operational protocol formalised by Ewertowski *et al.* (2019b) for low-cost UAV-SfM mapping of glacial landforms, and reproduces the geodetic survey design that Lamsters *et al.* (2022) successfully applied at Waldemarbreen, where two seasonal campaigns (2019 and 2021) yielded a mean surface lowering of −1.46 m at sub-decimetre ground sampling distance. The total RMSE of 3.36 cm (X 1.88 cm, Y 2.13 cm, Z 1.80 cm) achieved at Renardbreen sits well within the upper-bound uncertainty of those benchmark studies, so the threshold of geomorphic significance for the DoD can confidently be set at ±0.20 m. UAV products of this quality are now becoming the de facto reference standard for fine-scale geomorphological monitoring in the High Arctic; a closely related example along the adjacent Spitsbergen coast is provided by Czarnecki and Sobota (2025), who combined archival aerial photography (1966, 1990, 2017) with UAV surveys (2021–2022) to derive sub-decimetre DTMs and quantify multi-decadal shoreline retreat in the Kaffiøyra region. The principal trade-off is computational: the 11 467 images and >50 GB raw dataset processed here demonstrate that high-resolution coverage of even a relatively small (6 km^2) foreland is no longer the bottleneck.

In summary, the integration of decimetric UAV-SfM mapping with multi-temporal DoD analysis at Renardbreen yields three key insights. First, the modern frontal retreat rate (11.17 m yr^{-1}) is moderate by southern-Spitsbergen standards and consistent with a marine-to-land transition (Li *et al.* 2025). Second, the geomorphic budget of the foreland is dominated by fluvio-glacial reworking, with marginal accumulation, sandur incision and delta lobe reconfiguration recorded simultaneously (Bernard *et al.* 2017; Ewertowski *et al.* 2019a). Third, UAV-SfM products at 0.10 m px now resolve process signatures one order of magnitude below the regional landsystem mapping of McCerery *et al.* (2025), bridging the gap between site-scale geomorphology and archipelago-wide remote sensing.

Acknowledgements

This article was made possible by participation in the CRIOS project (Cryosphere of the Integrated Observatory Network in Svalbard). I would also like to thank the late Professor Piotr Zagórski for his support and for enabling my participation in the *31st Polar Expedition of UMCS*. I am also deeply grateful to three reviewers and to the handling editor for the time and care they devoted to this manuscript; their through and constructive comments greatly improved the paper and helped bring it to tis final form.

Supplementary materials. Supplementary figures S1 to S6, showing more detailed results, are available in Polish Polar DataBase at https://polar.cenagis.edu.pl/dataset/renard-glacier-proglacial-zone-uav-dem-orthophoto-2021-and-2023-supplementary-material.

References

Ballinger T.J., Overland J.E., Wang M., Bhatt U.S., Hanna E., Hanssen-Bauer I., Kim S.J., Thoman R.L. and Walsh J.E. 2020. Surface air temperature. *Arctic Report Card 2020*. NOAA, doi: 10.25923/gcw8-2z06.

Barry R.G. 2017. The Arctic cryosphere in the twenty-first century. *Geographical Review* 107: 69–88, doi: 10.1111/gere.12227.

Bartoszewski S. 1998. Runoff regime of rivers in Wedel Jarlsberg Land – Spitsbergen (in Polish). *Rozprawy habilitacyjne* LX. Wydział Biologii i Nauk o Ziemi, UMCS, Lublin: 1–167.

Bartoszewski S., Gluza A., Pękala K., Repelewska-Pękalowa J., Siwek K. and Zagórski P. 2003. The natural environment of Bellsund. *In:* Kostrzewski A. and Zwoliński Z. (eds.) *Functioning of ancient and modern geoecosystems of Spitsbergen*. Stowarzyszenie Geomorfologów Polskich, Poznań–Longyearbyen: 149–157 (in Polish).

Bernard E., Friedt J.M., Tolle F., Griselin M., Marlin C. and Prokop A. 2017. Investigating snowpack volumes and icing dynamics in the moraine of an Arctic catchment using UAV photogrammetry. *The Photogrammetric Record* 32: 497–512, doi: 10.11 11/phor.12217.

Birkenmajer K. 1972. Tertiary history of Spitsbergen and continental drift. *Acta Geologica Polonica* 22: 193–218.

Biskaborn B.K., Smith S.L., Noetzli J. *et al.* 2019. Permafrost is warming at a global scale. *Nature Communications* 10: 264, doi: 10.1038/s41467-018-08240-4.

Błaszczyk M., Jania J.A. and Kolondra L. 2013. Fluctuations of tidewater glaciers in Hornsund Fjord (Southern Svalbard) since the beginning of the 20th century. *Polish Polar Research* 34: 327–352, doi: 10.2478/popore-2013-0024.

Chandler B.M.P., Lovell H., Boston C.M. *et al*. 2018. Glacial geomorphological mapping: A review of approaches and frameworks for best practice. *Earth-Science Reviews* 185: 806–846, doi: 10.1016/j.earscirev.2018.07.015.

Czarnecki K. and Sobota I. 2025. UAV and photogrammetric techniques to study shoreline changes in the high Arctic as exemplified by the Kaffiøyra region, Svalbard. *Earth Surface Processes and Landforms* 50, doi: 10.1002/esp.70037.

Dobiński W. and Kasprzak M. 2022. Permafrost base degradation: characteristics and unknown threat with specific example from Hornsund, Svalbard. *Frontiers in Earth Science* 10: 802157, doi: 3389/feart.2022.802157.

Dudek J., Wieczorek I. and Strzelecki M.C. 2023. Paraglacial transformation and ice-dammed lake dynamics in a high Arctic glacier foreland, Gåsbreen, Svalbard. *Land Degradation & Development* 34: 4252–4271, doi: 10.1002/ldr.4773.

ESRI 2023. *Esri World imagery basemap. ArcGIS Online World Imagery*, https://services.arcgisonline.com/arcgis/rest/services/World_Imagery/MapServer.

Ewertowski M.W. and Śledź S. 2022. Evaluation of the influence of processing parameters in Structure-from-Motion software on the quality of digital elevation models and orthomosaics in the context of studies on Earth surface dynamics. *Remote Sensing* 14: 1312, doi: 10.3390/rs14061312.

Ewertowski M.W., Evans D.J.A., Roberts D.H., Tomczyk A.M., Ewertowski W. and Pleskot K. 2019a. Quantification of historical landscape change on the foreland of a receding polythermal glacier, Hørbyebreen, Svalbard. *Geomorphology* 325: 40–54, doi: 10.1016/j.geomorph.2018.09.027.

Ewertowski M.W., Tomczyk A.M., Evans D.J.A., Roberts D.H. and Ewertowski W. 2019b. Operational framework for rapid, very-high-resolution mapping of glacial geomorphology using low-cost unmanned aerial vehicles and Structure-from-Motion approach. *Remote Sensing* 11: 65, doi: 10.3390/rs11010065.

Johnson G.L. and Heezen B.C. 1967. Morphology and evolution of the Norwegian–Greenland Sea. *Deep Sea Research and Oceanographic Abstracts* 14: 755–771, doi: 10.1016/0011-7471(67)90011-9.

Kavan J. and Strzelecki M.C. 2023. Glacier decay boosts formation of new Arctic coastal environments – perspectives from Svalbard. *Land Degradation & Development* 34: 3467–3474, doi: 10.1002/ldr.4695.

Killingtveit Å., Pettersson L.-E. and Sand K. 2003. Water balance investigations in Svalbard. *Polar Research* 22: 161–174, doi: 10.1111/j.1751-8369.2003.tb00105.x.

Kostrzewski A. and Zwoliński Z. 2013. Polish geomorphological research on Spitsbergen. In: Zwoliński Z., Kostrzewski A. and Pulina M. (eds.), *Ancient and modern geoecosystems of Spitsbergen. Polish geomorphological research*. Bogucki Wydawnictwo Naukowe, Poznań: 11–17 (in Polish).

Lamsters K., Karušs J., Džeriņš P., Sobota I. and Ješkins J. 2022. Surface characteristics, elevation change, and velocity of high-Arctic valley glacier from repeated high-resolution UAV photogrammetry. *Remote Sensing* 14: 1029, doi: 10.3390/rs14041029.

Li T., Hofer S., Moholdt G., Igneczi A., Heidler K., Zhu X.X. and Bamber J.L. 2025. Pervasive glacier retreats across Svalbard from 1985 to 2023. *Nature Communications* 16: 705, doi: 10.1038/s41467-025-55948-1.

McCerery R., Davies B.J., Lovell H., Calvo-Ryan R., Pearce D. A., Małecki J. and Woodward J. 2025. Landsystem models from remote and field-based geomorphological mapping reveal diverse glacier dynamics on Svalbard. *Geomorphology* 48: 4109854, doi: 10.1016/j.geomorph.2025.109854.

Mercier D. and Laffly D. 2005. Actual paraglacial progradation of the coastal zone in the Kongsfjorden area, western Spitsbergen, Svalbard. *In:* Harris C. and Murton J.B. (eds.), *Cryospheric Systems: Glaciers and Permafrost*. *Geological Society of London Special Publications* 242: 111–117, doi: 10.1144/GSL.SP.2005.242.01.10.

Pękala K., Repelewska-Pękalowa J., Bartoszewski S. *et al.* 2013. Geographical environment in the vicinity of the Maria Curie-Skłodowska University expedition base – Calypsobyen. *In:* Zwoliński Z., Kostrzewski A. and Pulina M. (eds.) *Ancient and modern geoecosystems of Spitsbergen. Polish geomorphological research*. Bogucki Wydawnictwo Naukowe, Poznań (in Polish).

Rachlewicz G. 2009. *Contemporary sediment fluxes and relief changes in high Arctic glacierized valley systems, Billefjorden, Central Spitsbergen*. Wydawnictwo Naukowe, Seria Geografia 87, UAM, Poznań.

Reder J. 1996. Evolution of marginal zones during glacial retreat in northwestern Wedel Jarlsberg Land, Spitsbergen. *Polish Polar Research* 17: 61–84.

Reder J. and Zagórski P. 2007. Recession and development of the marginal zone of the Scott Glacier (geomorphology of the southern side of Bellsund). *Landform Analysis* 5: 175–178.

Stankowski W.T.J., Bartoszewski S., Birkenmajer K., Borsiak J., Bukowska-Jania E., Karczewski A., Skiba S. and Zwoliński Z. 2013. Geographical environment of Spitsbergen. *In:* Zwoliński Z., Kostrzewski A. and Pulina M. (eds.) *Ancient and modern geoecosystems of Spitsbergen. Polish geomorphological research*. Bogucki Wydawnictwo Naukowe, Poznań: 19–21 (in Polish).

Strzelecki M.C., Long A.J., Lloyd J.M., Małecki J., Zagórski P., Pawłowski Ł. and Jaskólski M.W. 2018. The role of rapid glacier retreat and landscape transformation in controlling the post-Little Ice Age evolution of paraglacial coasts in central

Spitsbergen, Billefjorden, Svalbard. *Land Degradation & Development* 29: 1962–1978, doi: 10.1002/ldr.2923.

Strzelecki M.C., Szczuciński W., Dominiczak A., Zagórski P., Dudek J. and Knight J. 2020. New fjords, new coasts, new landscapes: the geomorphology of paraglacial coasts formed after recent glacier retreat in Brepollen (Hornsund, southern Svalbard). *Earth Surface Processes and Landforms* 45: 1325–1334, doi: 1002/esp.4819.

Sumata H., de Steur L., Divine D.V., Granskog M.A. and Gerland S. 2023. Regime shift in Arctic Ocean sea ice thickness. *Nature* 615: 443–449, doi: 10.1038/s41586-022-05686-x.

Szczęsny R., Dzierżek J., Harasimiuk M., Nitychoruk J., Pękala K. and Repelewska-Pękalowa J. 1989. *Photogeological map of the Renardbreen, Scottbreen and Blomlibreen forefield (Wedel Jarlsberg Land, Spitsbergen)*, scale 1:10 000. Wydawnictwa Geologiczne, Warszawa.

Śledź S., Ewertowski M.W. and Piekarczyk J. 2021. Applications of unmanned aerial vehicle (UAV) surveys and Structure-from-Motion photogrammetry in glacial and periglacial geomorphology. *Geomorphology* 378: 107620, doi: 10.1016/j.geomorph.2021.107620.

Tonkin T.N. and Midgley N.G. 2016. Ground-control networks for image-based surface reconstruction: an investigation of optimum survey designs using UAV-derived imagery and Structure-from-Motion photogrammetry. *Remote Sensing* 8: 786, doi: 10.3390/rs8090786.

Walczowski W. and Piechura J. 2011. Influence of the West Spitsbergen Current on the local climate. *International Journal of Climatology* 31: 1088–1093, doi: 10.1002/ joc. 2338.

Zagórski P. 2011. Shoreline dynamics of Calypsostranda (NW Wedel Jarlsberg Land, Svalbard) during the last century. *Polish Polar Research* 32: 67–99.

Zagórski P., Siwek K. and Gluza A. 2008. Changes in the extent of the front and geometry of the Renard Glacier (Spitsbergen) against the background of climatic fluctuations in the 20th century. *Problemy Klimatologii Polarnej* 18: 113–125 (in Polish).

Zagórski P., Gajek G. and Demczuk P. 2012. Influence of glacier systems on the functioning of the coastal zone of Recherchefjorden (Svalbard). *Zeitschrift für Geomorphologie, Supplementary Issues* 56: 101–122, doi: 10.1127/0372-8854/2012/S-00075.